Advances in Structural Engineering

Advances in Structural Engineering
2024, Vol. 0(0) 1–21

DOI: 10.1177/13694332241242984
journals.sagepub.com/home/ase
Sage

Substructural damage identification in a digital twin framework using heterogeneous response reconstruction

Guangcai Zhang[1], Zhenwei Zhou[2], Chunfeng Wan[1], Zhenghao Ding[3], Zhishen Wu[1], Liyu Xie[4] and Songtao Xue[4,5]

Abstract

The external excitations, interface forces and responses at the interface degrees-of-freedom are normally required in many existing substructural condition assessment methods, while they are difficult or even impossible to be accurately measured. To address this issue, a digital twin framework for output-only substructural damage identification with data fusion of muti-type responses is proposed in the present paper. First, heterogeneous responses including displacements, strains and accelerations from the target substructure are measured and divided into two sets. The multi-type responses in measurement set 2 are reconstructed with the first set of responses and transmissibility matrix in time domain. Then, a recovery method is introduced to obtain angular displacements from translational displacements and strains, to acquire angular accelerations from translational accelerations and the second order derivatives of strains by continuous wavelet transform. The recovered angular displacements and angular accelerations are involved into the evaluation of objective function. Besides, to avoid the single and monotonous search operation of traditional optimization algorithms, a reinforced learning-assisted Q-learning hybrid evolutionary algorithm (QHEA) by integrating Q-learning algorithm, differential evolution algorithm, Jaya algorithm, is developed as a search tool to solve the optimization-based inverse problem. The most suitable search strategy among DE/rand/1, DE/rand/2, DE/current-to-best/1, Jaya mutation in each iteration is selected and implemented under the guidance of Q-learning algorithm. Numerical studies on a three-span beam structure are performed to verify the effectiveness of the proposed approach. The results demonstrates that the proposed output-only substructural damage identification approach can accurately identify locations and severities of multiple damages even with high noise-polluted responses.

Keywords

damage identification, digital twin, continuous wavelet transform, response reconstruction, evolutionary algorithm, substructure

Introduction

Over the past few decades, in view of the advance of new materials and structures (Elshazli et al., 2022; Jiang et al., 2022; Wilt et al., 2023), various vibration-based structural damage identification approaches, or acoustic emission techniques have been developed and employed, and fruitful research results are achieved (Ai et al., 2022, 2023a, 2023b, 2024; Ding et al., 2019; Doebling et al., 1998; Feng et al., 2021; Hou et al., 2020; Li et al., 2013, 2022; Zhang et al., 2023b). Mathematically, structural identification can be formulated as a constrained optimization inverse problem in which the objective function is defined as the discrepancy between the measured and the simulated responses.

The inverse identification could be properly addressed by minimizing the objective function using diverse swarm

[1]Key Laboratory of Concrete and Prestressed Concrete Structure of Ministry of Education, Southeast University, Nanjing, China
[2]School of Civil Engineering and Architecture, East China Jiaotong University, Nanchang, China
[3]JSPS International Research Fellow, Division of Environmental Science and Technology, Kyoto University, Kyoto, Japan
[4]Department of Disaster Mitigation for Structures, Tongji University, Shanghai, China
[5]Department of Architecture, Tohoku Institute of Technology, Sendai, Japan

Corresponding authors:
Chunfeng Wan, Key Laboratory of Concrete and Prestressed Concrete Structure of Ministry of Education, Southeast University, No. 2, Southeast University Road, Jiangning District, Nanjing 211189, China.
Email: wan@seu.edu.cn

Zhishen Wu, School of Civil Engineering, Southeast University, No. 2, Southeast University Road, Jiangning District, Nanjing 211189, China.
Email: zswu@seu.edu.cn

Songtao Xue, Department of Disaster Mitigation for Structures, Tongji University, No. 1239, Siping Road, Shanghai 200092, China.
Email: xue@tongji.edu.cn

intelligence algorithms, such as genetic algorithm, grey wolf optimizer, particle swarm optimization algorithm, cuckoo search algorithm, whale optimization algorithm, Jaya algorithm (Rao, 2016). Among these algorithms, Jaya algorithm receives increasing attention owing to its merits of simple structure and without any algorithm-specific parameters, but it suffers by the problems of slow convergence speed and easy to be trapped into local optimal solution. With the purpose of improving the performance of basic Jaya algorithm, the Hooke–Jeeves local pattern search (Ding et al., 2022) or Tree Seeds Algorithm (Ding et al., 2020) is introduced into standard Jaya algorithm. In this study, a new optimization algorithm, named Q-learning hybrid evolutionary algorithm (QHEA) is developed by integrating Jaya algorithm, differential algorithm and Q-learning algorithm. For each individual in the population, the proposed QHEA could choose the most suitable operation adaptively and continuously from search strategy pool, i.e., DE/rand/1, DE/rand/2, DE/current-to-best/1 and Jaya mutation under the guidance of the Q-learning during iterations, which enable a better balance between the exploration capability and exploitation capability.

Nevertheless, there are still some issues that have not been properly addressed in previous researches, which limits their practical applications in damage identification. First, measurements of external excitation are required and treated as input in many structural identification methods. In practice, it is difficult or even impossible to directly acquire excitation data, for example, wind load, seismic load, and traffic load (Zhang et al., 2022). Engineering structures usually have hundreds of degrees of freedom, but only partial output responses can be obtained. Incomplete information poses a huge challenge for traditional identification methods. Second, the majority of studies on structural identification employs a single type of measurement. Heterogeneous sensors, e.g., displacement transducers, strain gauges, accelerometers, are usually used in structural health monitoring system, so it is necessary to develop data fusion technique to effectively combine their individual characteristics. Third, the low computational efficiency and poor convergence of global methods discourage the use for large-scale and complex structural systems considering substantial variables to be identified.

For addressing the first challenge, namely, identifying structural damages without measurement of excitation forces, some output-only identification methods have been developed. For example, a synergy of a modified Newmark integration scheme for force identification and a hybrid artificial bee colony algorithm for parameter identification was proposed (Sun and Betti, 2014). Similarly, an iterative identification strategy, combining Tikhonov regularization method for force identification meanwhile modified Jaya algorithm (Zhang et al., 2023a) or dynamic hybrid quantum particle swarm optimizer (Jayalakshmi et al., 2018) for structural parameter identification was introduced. It is noted that the simultaneous identification of unknown structural parameters and input force may further induce the ill-posedness of the inverse problem. In addition, damages and input force are iteratively identified at each time step, which would necessarily consume considerable computational resources, especially for complex and large-scale structures (Zhu et al., 2014). Response reconstruction technique provides an alternative approach for the absence of excitation measurements, acquired good performance (Zhu et al., 2023). Zhang and Xu (2017) proposed a multi-level damage identification method using the Kalman filter-based response reconstruction. Besides, response reconstruction methods based on the transmissibility concept have been proposed and applied into damage detection in the frequency-domain (Law et al., 2011), wavelet-domain (Li and Hao, 2014), state space domain (Zhang et al., 2020), time-domain (Zou et al., 2022).

For addressing the second challenge, namely, some effort has been devoted to structural health monitoring with multi-type sensors (strain gauges, displacement transducers, accelerometers, etc.) These measurements have their own advantages and drawbacks, and they could provide comprehensive information about the structure's condition. The merits of incorporating heterogeneous data fusion for better monitoring have been demonstrated (Yang et al., 2023). For instance, Sun and Büyüköztürk (2015) fused acceleration, displacement and strain time histories through a state space model for force identification, and validated the effectiveness with a numerical truss bridge. Kim et al. (2014) presented a dynamic displacement estimation method based on multi-rate Kalman filtering using acceleration and intermittent displacement measurements. Yu et al. (2023) combined initial diagnosis results from each sensor via Dempster-Shafer fusion algorithm for condition assessment of concrete arch beam. Experimental test on a Sydney Harbour Bridge in laboratory indicated the accuracy of multi-sensor fusion for structural damage diagnosis. Zhang and Xu (2016) proposed a new multi-sensing damage identification method using optimal sensor placement and Kalman filter-based response reconstruction. Numerical and experimental studies showed that fusion of heterogeneous measurements can achieve more superior performance than single-type responses on the equivalent locations.

For addressing the third challenge, substructural identification methods (Weng et al., 2020) was developed to identify damages by dividing a large-scale structure into several substructures instead of in a global manner. In fact, substructural identification methods based on the "divide-and-conquer" strategy can significantly improve

computational efficiency and accuracy since the dimensions of the unknown parameters are reduced. For example, Tee et al. (2009) presented a substructural strategy for identification of stiffness damage with incomplete measurement. Li et al. (2012) adopted a response reconstruction method to detect substructural damage in frequency domain, and verified its performance using experimental tests on a steel frame structure. Liu et al. (2015) proposed a substructural identification method considering the interface force sensitivity. The unknown interface forces were identified using the Newmark method. Ni et al. (2023) developed a new response reconstruction technique in time domain and combined it with the Bayesian inference method for probabilistic model updating of the target substructure. Li and Sun (2024) utilized the transmissibility function as a damage indicator to detect and localize the substructural damages. Nevertheless, the potentials of utilizing heterogeneous response reconstruction for substructural damage identification have not been well explored.

With the advance of artificial intelligence, measurement techniques, internet of things, etc., the digital twin concept applied in various real-world engineering fields, such as industrial manufacturing (Tao et al., 2018), infrastructure health monitoring and management (Liu et al., 2023), structural fatigue life prediction (Wang et al., 2022), smart cities and urban spaces (Torzoni et al., 2024), have attracted much attentions. In recent years, some digital twin conceptual framework in the context of structural health monitoring have been developed (Teng et al., 2023; Wang et al., 2021). It is known that damage identification is the core problem and an essential module in the digital twin-based health monitoring framework. Wang et al. (2023) proposed a novel digital twin framework for damage detection of offshore jacket platforms considering optimal sensor placement. Ritto and Rochinha (2021) combined the physics-based model and machine learning as a digital twin to detect damages. Teng et al. (2023) identified damages of the real bridge structure by utilizing digital twin technology to generate a large number of damage samples so as to train a convolutional neural network. The results showed the proposed method can significantly improve the identification accuracy of bridge model.

For properly addressing aforementioned challenges, in this work, a digital twin framework for output-only substructural damage identification with data fusion of mutitype responses is proposed, as is shown in Figure 1. It is noticed that this framework consists of four diffident models, i.e., a physical model, a virtual model, a dynamic responses reconstruction model and a damage identification model. The physical three-span beam structure is termed as the basis of constructing the digital twin virtual model. In the virtual model, muti-type dynamic responses are obtained by implementing simulations considering different damaged cases, noise levels, modeling errors, number of sensors, etc. The dynamic responses reconstruction model seeks to reconstruct multi-sensing responses of civil structures at locations where no sensors

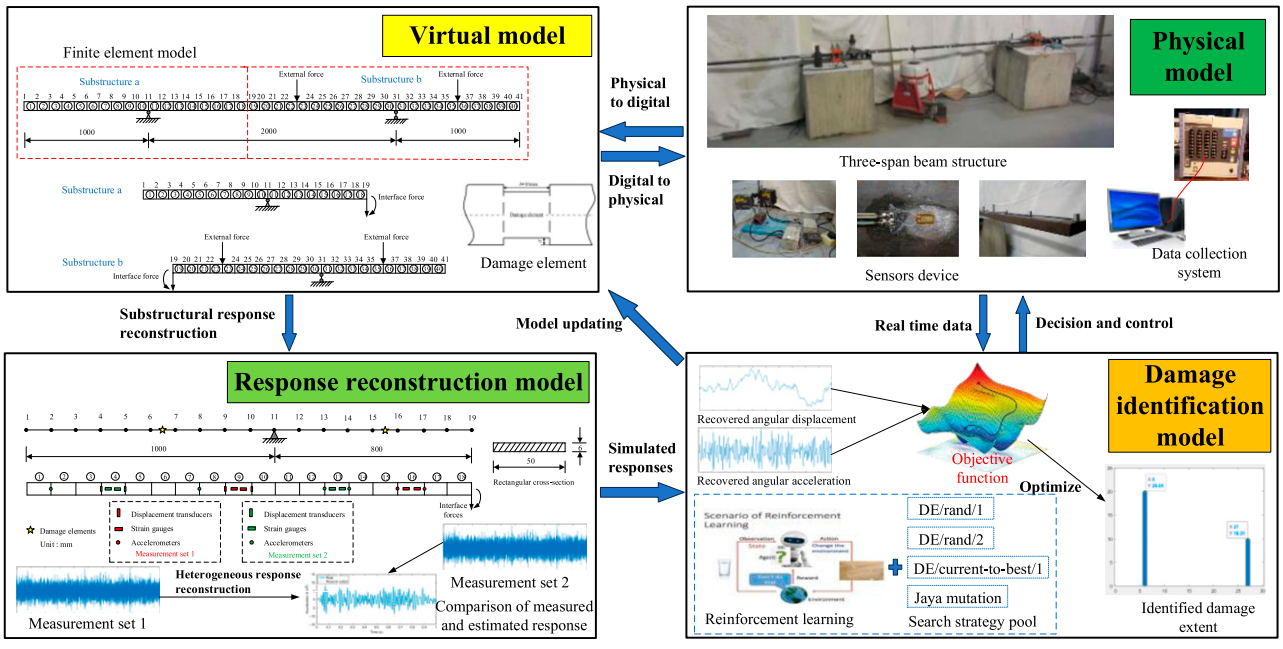

Figure 1. The proposed substructural damage identification method in a digital twin framework.

installed based on the proposed heterogeneous response reconstruction technique and recovery method. More specifically, muti-type responses (displacements, strains, accelerations, etc.,) from the target substructure with preinstalled sensors (displacement transducers, strain gauges, accelerometers, etc.,) are divide into two measurement sets, i.e., set 1 and set 2. Dynamic responses in a substructure are reconstructed by transforming the measured responses of set 1 into responses of set 2 with the transmissibility matrix in time domain. The measured responses from the real structure model and simulated responses from the response reconstruction model are feed into the damage identification model, and they are used to established an objective function, optimized by the proposed a new heuristic algorithm, Q-learning hybrid evolutionary algorithm. Structural parameters are updated until the possible damage locations and severities are detected, which is crucial for structural degradation evaluation, safety alarm, and maintenance operations. The dynamic responses reconstruction model and the damage identification model are detailed described, respectively.

Dynamic response reconstruction model for substructure

The equation of motion for a multi-DOF dynamic system subjected to external forces can be expressed as

$$M\ddot{u}(t) + C\dot{u}(t) + Ku(t) = Bf(t) \tag{1}$$

where M, C, K stand for the structural mass, damping and stiffness matrices, respectively; $\ddot{u}(t)$, $\dot{u}(t)$ and $u(t)$ represent the acceleration, velocity and displacement responses of the dynamic system, respectively; $f(t)$ means the external forces applied to the structure and B maps the force location to its associated DOFs. Structural dynamic responses (acceleration, velocity, displacement, etc.,) can be obtained by solving equation (1) with the Newmark-β method. Rayleigh damping model is used as $C = \zeta_1 M + \zeta_2 K$, where ζ_1 and ζ_2 stand for two damping coefficients.

Herein, a three-span beam structure is studied, As shown in Figure 2(a). The whole structure is divided into two substructures, namely, substructure a on the left side and substructure b on the right side.

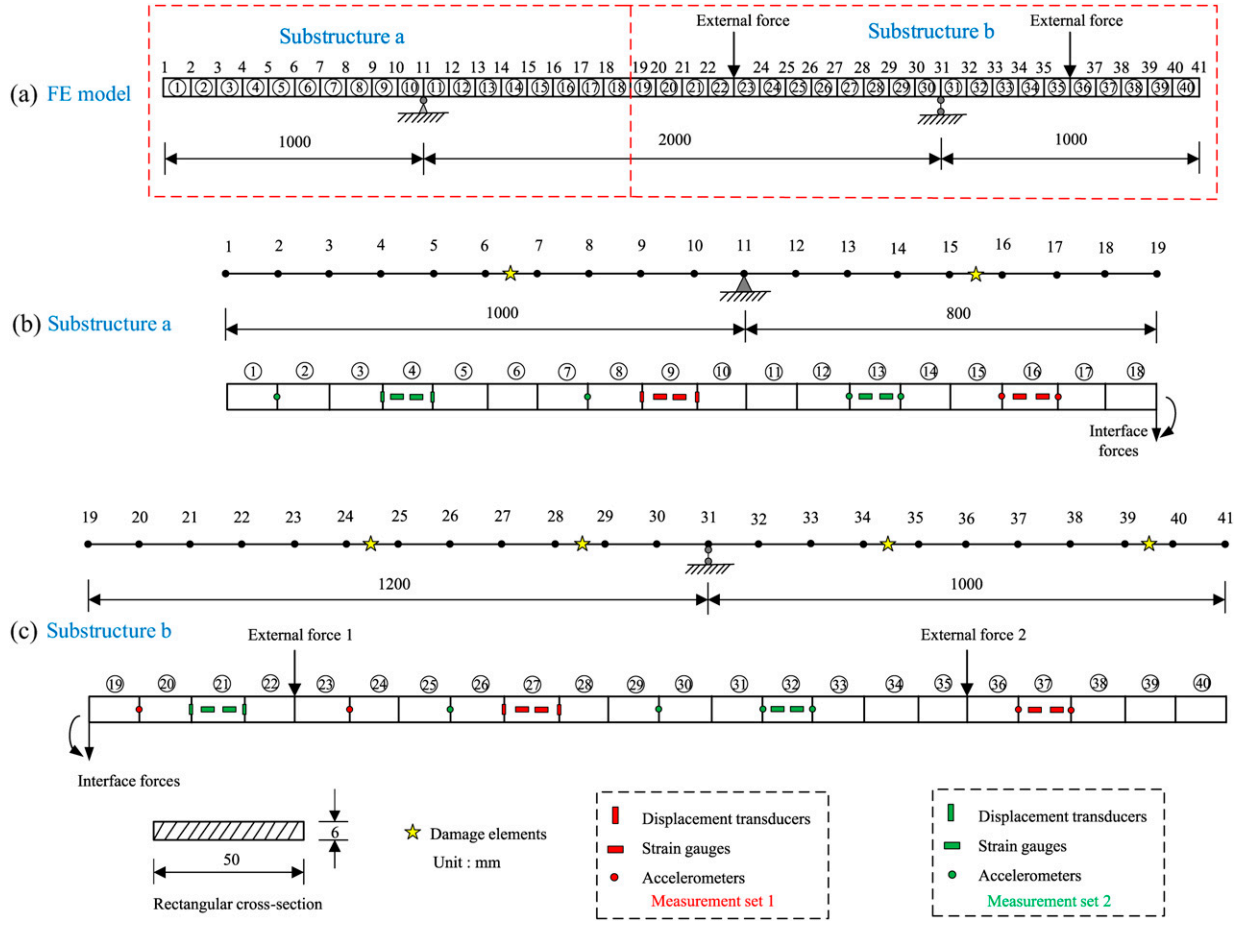

Figure 2. Three-span beam structure: (a) FE model; (b) substructure *a*; (c) substructure *b*.

By equation (1), the equation of motion can be rewritten as follows

$$\begin{bmatrix} M_{aa} & M_{ab} \\ M_{ba} & M_{bb} \end{bmatrix} \begin{bmatrix} \ddot{u}_a(t) \\ \ddot{u}_b(t) \end{bmatrix} + \begin{bmatrix} C_{aa} & C_{ab} \\ C_{ba} & C_{bb} \end{bmatrix} \begin{bmatrix} \dot{u}_a(t) \\ \dot{u}_b(t) \end{bmatrix} + \begin{bmatrix} K_{aa} & K_{ab} \\ K_{ba} & K_{bb} \end{bmatrix} \begin{bmatrix} u_a(t) \\ u_b(t) \end{bmatrix} = \begin{bmatrix} 0 \\ Bf(t) \end{bmatrix} \tag{2}$$

In Figure 2(b), obviously, the external force is outside the substructure a. Treating the interface forces as input, the equation of motion substructure a is expressed as

$$M_{aa}\ddot{u}_a(t) + C_{aa}\dot{u}_a(t) + K_{aa}u_a(t) = B_a g_a(t) \tag{3}$$

where $g_a(t)$ denotes the vector of interface forces and B_a is the mapping matrix associated with the force location.

Similarly, the equation of motion substructure b subjected to external forces and interface forces can be expressed as

$$M_{bb}\ddot{u}_b(t) + C_{bb}\dot{u}_b(t) + K_{bb}u_b(t) = B_b[g_b(t) \quad f(t)]^T \tag{4}$$

where $g_b(t)$ denotes the vector of interface forces; B_b is the mapping matrix associated with the location of all input forces.

The external force outside the substructure

For substructure a, the external force is outside the substructure, which is analyzed as the first case. In fact, multiple types of sensors are usually installed on the target civil structure, e.g., displacement transducers, fiber Bragg grating strain sensors, and accelerometers. In this end, heterogeneous measurements, displacements, strains, accelerations, etc., are recorded to evaluate the healthy condition of major infrastructures. In consideration of superposition theory, the displacement response $u_p(t_n)$, strain response $\varepsilon_q(t_n)$, acceleration response $\ddot{u}_s(t_n)$ of substructure a from the p-th, q-th and s-th DOFs at time t_n can be written as

$$u_p(t_n) = u_{p,1}(t_n) + u_{p,2}(t_n) + , ..., + u_{p,nf}(t_n) = \sum_{i=1}^{nf} u_{p,i}(t_n) \tag{5a}$$

$$\varepsilon_q(t_n) = \varepsilon_{q,1}(t_n) + \varepsilon_{q,2}(t_n) + , ..., + \varepsilon_{q,nf}(t_n) = \sum_{i=1}^{nf} \varepsilon_{q,i}(t_n) \tag{5b}$$

$$\ddot{u}_s(t_n) = \ddot{u}_{s,1}(t_n) + \ddot{u}_{s,2}(t_n) + , ..., + \ddot{u}_{s,nf}(t_n) = \sum_{i=1}^{nf} \ddot{u}_{s,i}(t_n) \tag{5c}$$

where nf means the number of unknown interface forces.

The displacement response $u_{p,i}(t_n)$, acceleration response $\ddot{u}_{s,i}(t_n)$ at instant t_n under the i-th interface excitation $g_{a,i}$ can be expressed as

$$u_{p,i}(t_n) = \int_0^{t_n} h_{p,i}(t_n - \tau) g_{a,i}(\tau) d\tau \tag{6a}$$

$$\ddot{u}_{s,i}(t_n) = \int_0^{t_n} \ddot{h}_{s,i}(t_n - \tau) g_{a,i}(\tau) d\tau \tag{6b}$$

where $h_{p,i}(t_n - \tau)$ and $\ddot{h}_{s,i}(t_n - \tau)$ are the unit impulse response function of displacement and acceleration, respectively.

According to the displacement-strain relation, strain response $\varepsilon_{q,i}(t_n)$ can be obtained as

$$\varepsilon_{q,i}(t_n) = \int_0^{t_n} [z_1 \quad \cdots \quad z_{ndof}][h_{ds,i}(t_n - \tau) \quad \cdots \quad h_{de,i}(t_n - \tau)]^T g_{a,i}(\tau) d\tau = \int_0^{t_n} h_{q,i}^{\varepsilon}(t_n - \tau) g_{a,i}(\tau) d\tau \tag{7}$$

where $ndof$ denotes the number of DOFs of an element; subscripts ds and de stand for the degrees of freedom to start and end. For the purpose of simplifying expression, strain response is $\varepsilon_{q,i}(t_n) = \int_0^{t_n} h_{q,i}^{\varepsilon}(t_n - \tau) g_{a,i}(\tau) d\tau$.

By equations (5a), (5b), (5c)–(7), it can be given as

$$u_p(t_n) = \sum_{i=1}^{nf} \int_0^{t_n} h_{p,i}(t_n - \tau) g_{a,i}(\tau) d\tau \tag{8a}$$

$$\varepsilon_q(t_n) = \sum_{i=1}^{nf} \int_0^{t_n} h_{q,i}^{\varepsilon}(t_n - \tau) g_{a,i}(\tau) d\tau \tag{8b}$$

$$\ddot{u}_s(t_n) = \sum_{i=1}^{nf} \int_0^{t_n} \ddot{h}_{s,i}(t_n - \tau) g_{a,i}(\tau) d\tau \tag{8c}$$

Then, equations (8a)–(8c) can be rewritten in discretized form as follows

$$u_p(t_n) = \sum_{i=1}^{nf} h_{p,i}(t_n) g_{a,i}(t_n) \tag{9a}$$

$$\varepsilon_q(t_n) = \sum_{i=1}^{nf} h_{q,i}^{\varepsilon}(t_n) g_{a,i}(t_n) \tag{9b}$$

$$\ddot{u}_s(t_n) = \sum_{i=1}^{nf} \ddot{h}_{s,i}(t_n) g_{a,i}(t_n) \tag{9c}$$

The equation of motion of the target substructure a under the unit impulse excitation is

$$M_{aa}\ddot{h}_a(t) + C_{aa}\dot{h}_a(t) + K_{aa}h_a(t) = B_a\delta(t) \tag{10}$$

where $\delta(t)$ is the Dirac delta function.

The unit impulse response functions can be calculated by following Newmark-β method

$$\begin{cases} M_{aa}\ddot{h}_a(t) + C_{aa}\dot{h}_a(t) + K_{aa}h_a(t) = 0 \\ h_a(0) = 0, \dot{h}_a(0) = {M_{aa}}^{-1}B_a \end{cases} \tag{11}$$

By equations (9a)–(9c), the dynamic displacement, strain and acceleration responses of the substructure a can be represented as

$$Y_u = \sum_{i=1}^{nf} H_{u,i}g_{a,i},\ Y_\varepsilon = \sum_{i=1}^{nf} H_{\varepsilon,i}g_{a,i},\ Y_{\ddot{u}} = \sum_{i=1}^{nf} H_{\ddot{u},i}g_{a,i} \tag{12}$$

where $Y_u = [Y_{u_1}, Y_{u_2}, ..., Y_{u_n}]^T$, $Y_\varepsilon = [Y_{\varepsilon_1}, Y_{\varepsilon_2}, ..., Y_{\varepsilon_n}]^T$, $Y_{\ddot{u}} = [Y_{\ddot{u}_1}, Y_{\ddot{u}_2}, ..., Y_{\ddot{u}_n}]^T$; u_n ε_n, $\ddot{u}_n$ stand for the number of displacement transducers, strain sensors, accelerometers, respectively; $H_{u,i} = [H_{u_1,i}, H_{u_2,i}, ..., H_{u_n,i}]^T$, $H_{\varepsilon,i} = [H_{\varepsilon_1,i}, H_{\varepsilon_2,i}, ..., H_{\varepsilon_n,i}]^T$, $H_{\ddot{u},i} = [H_{\ddot{u}_1,i}, H_{\ddot{u}_2,i}, ..., H_{\ddot{u}_n,i}]^T$, their explicit expression can be given as

$$H_{u_n,i} = \begin{bmatrix} h_{u_n,i}(t_0) & 0 & 0 & 0 & 0 \\ h_{u_n,i}(t_1) & h_{u_n,i}(t_0) & 0 & 0 & 0 \\ h_{u_n,i}(t_2) & h_{u_n,i}(t_1) & h_{u_n,i}(t_0) & 0 & 0 \\ \vdots & \vdots & \vdots & \ddots & \vdots \\ h_{u_n,i}(t_n) & h_{u_n,i}(t_{n-1}) & h_{u_n,i}(t_{n-2}) & \cdots & h_{u_n,i}(t_0) \end{bmatrix} \tag{13a}$$

$$H_{\varepsilon_n,i} = \begin{bmatrix} h^{\varepsilon}_{\varepsilon_n,i}(t_0) & 0 & 0 & 0 & 0 \\ h^{\varepsilon}_{\varepsilon_n,i}(t_1) & h^{\varepsilon}_{\varepsilon_n,i}(t_0) & 0 & 0 & 0 \\ h^{\varepsilon}_{\varepsilon_n,i}(t_2) & h^{\varepsilon}_{\varepsilon_n,i}(t_1) & h^{\varepsilon}_{\varepsilon_n,i}(t_0) & 0 & 0 \\ \vdots & \vdots & \vdots & \ddots & \vdots \\ h^{\varepsilon}_{\varepsilon_n,i}(t_n) & h^{\varepsilon}_{\varepsilon_n,i}(t_{n-1}) & h^{\varepsilon}_{\varepsilon_n,i}(t_{n-2}) & \cdots & h^{\varepsilon}_{\varepsilon_n,i}(t_0) \end{bmatrix} \tag{13b}$$

$$H_{\ddot{u}_n,i} = \begin{bmatrix} \ddot{h}_{\ddot{u}_n,i}(t_0) & 0 & 0 & 0 & 0 \\ \dot{h}_{\ddot{u}_n,i}(t_1) & \ddot{h}_{\ddot{u}_n,i}(t_0) & 0 & 0 & 0 \\ \dot{h}_{\ddot{u}_n,i}(t_2) & \dot{h}_{\ddot{u}_n,i}(t_1) & \ddot{h}_{\ddot{u}_n,i}(t_0) & 0 & 0 \\ \vdots & \vdots & \vdots & \ddots & \vdots \\ \dot{h}_{\ddot{u}_n,i}(t_n) & \dot{h}_{\ddot{u}_n,i}(t_{n-1}) & \dot{h}_{\ddot{u}_n,i}(t_{n-2}) & \cdots & \dot{h}_{\ddot{u}_n,i}(t_0) \end{bmatrix} \tag{13c}$$

The dimensions of Y_u, Y_ε, $Y_{\ddot{u}}$ are $(u_n \times t_n) \times 1$, $(\varepsilon_n \times t_n) \times 1$, $(\ddot{u}_n \times t_n) \times 1$. The dimensions of H_u, H_ε, $H_{\ddot{u}}$ are $(u_n \times t_n) \times (nf \times t_n)$, $(\varepsilon_n \times t_n) \times (nf \times t_n)$, $(\ddot{u}_n \times t_n) \times (nf \times t_n)$. In consideration of the huge magnitude difference between heterogenous responses, three rescaling parameters are introduced to rescale these data as follows

$$\tilde{Y}_u = \gamma_u Y_u = \gamma_u \sum_{i=1}^{nf} H_{u,i}g_{a,i} = \sum_{i=1}^{nf} \tilde{H}_{u,i}g_{a,i} \tag{14a}$$

$$\tilde{Y}_\varepsilon = \gamma_\varepsilon Y_\varepsilon = \gamma_\varepsilon \sum_{i=1}^{nf} H_{\varepsilon,i}g_{a,i} = \sum_{i=1}^{nf} \tilde{H}_{\varepsilon,i}g_{a,i} \tag{14b}$$

$$\tilde{Y}_{\ddot{u}} = \gamma_{\ddot{u}} Y_{\ddot{u}} = \gamma_{\ddot{u}} \sum_{i=1}^{nf} H_{\ddot{u},i}g_{a,i} = \sum_{i=1}^{nf} \tilde{H}_{\ddot{u},i}g_{a,i} \tag{14c}$$

where γ_u, γ_ε, $\gamma_{\ddot{u}}$ are the rescaling parameters corresponding to displacement, strain and acceleration measurements, and their values can be determined by $\gamma_u = \|Y_u\|_2^{-1}, \gamma_\varepsilon = \|Y_\varepsilon\|_2^{-1}, \gamma_{\ddot{u}} = \|Y_{\ddot{u}}\|_2^{-1}$.

By the above equations (14a)–(14c), the assembled expression of heterogeneous measurements (displacement, strain, acceleration) could be shown as

$$Y = Hg_a \tag{15}$$

where assembled Y and H are

$$Y = \left[\tilde{Y}_u, \tilde{Y}_\varepsilon, \tilde{Y}_{\ddot{u}}\right]^T, H = \left[\tilde{H}_u, \tilde{H}_\varepsilon, \tilde{H}_{\ddot{u}}\right]^T \tag{16}$$

In equation (15), the relationship between the rescaled heterogeneous measurements Y and interface forces g_a is given. In this study, different from the response reconstruction technique in previous Refs. (Law et al., 2011; Li and Hao, 2014), a new heterogeneous response reconstruction technique is proposed for substructural damage identification with multiple-type sensors. The measured heterogeneous responses in damaged state from the target substructure a are divided into two sets, namely, measurement set 1 Y_{mea}^{set1} and measurement set 2 Y_{mea}^{set2}, and they can be defined as

$$\begin{cases} Y_{mea}^{set1} = H_1 g_a \\ Y_{mea}^{set2} = H_2 g_a \end{cases} \tag{17}$$

where $H_1 = [H_{1,1}, H_{1,2}, ..., H_{1,nf}]$, $H_2 = [H_{2,1}, H_{2,2}, ..., H_{2,nf}]$, $g_a = [g_{a,1}, g_{a,2}, ..., g_{a,nf}]^T$.

Then, the reconstructed responses of measurement set 2 Y_{rec}^{set2} can be obtained from the measurement set 1 as

$$Y_{rec}^{set2} = H_2(H_1)^+ Y_{mea}^{set1} \tag{18}$$

where $(H_1)^+$ denotes the pseudo-inverse of the matrix H_1; transformation matrix $T_{12} = H_2(H_1)^+$.

It is noted that there is no specific requirement to divide measured responses into two sets, but the number of measurements in the first set should not be less than the number of unknown interface forces to ensure the unique solution in equation (18).

The external force within the substructure

As shown in Figure 2(c), the substructure b is subject to both the external excitations f_E and the interface forces g_b from adjacent substructure a. The heterogeneous responses of the substructure b can be obtained in a form similar to equation (15) as follows

$$Y = H_I g_b + H_E f_E \tag{19}$$

where H_I and H_E represent the impulse response function matrices of the substructure b associated with the interface forces and external forces, respectively.

Equation (19) can be further simplified as

$$Y = \overline{H}F \tag{20}$$

where $\overline{H} = [H_I, H_E]$, $F = [g_b, f_E]^T$.

According to the theory of response reconstruction technique, the measured heterogeneous responses in damaged state from the target substructure b are divided into two sets, namely, measurement set 1 Y_{mea}^{set1} and measurement set 2 Y_{mea}^{set2}, and they can be given as

$$\begin{cases} Y_{mea}^{set1} = \overline{H}_1 F \\ Y_{mea}^{set2} = \overline{H}_2 F \end{cases} \tag{21}$$

The reconstructed responses of measurement set 2 Y_{rec}^{set2} can be calculated by following equation when the numbers of measurements set 1 are not less than the number of both the external forces and interface forces on the substructure b

$$Y_{rec}^{set2} = \overline{H}_2 (\overline{H}_1)^+ Y_{mea}^{set1} \tag{22}$$

where transmissibility matrix is $T_{12} = \overline{H}_2 (\overline{H}_1)^+$.

In general, the problem of solving the equation (18) or equation (22) is an ill-posed inverse problem. Disappointing estimation results may be acquired if taking the measurement noise into consideration. Accordingly, Tikhonov regularization method is utilized to obtain a bounded solution as follows

$$F = \left(\overline{H}_1^T \overline{H}_1 + \lambda I\right)^{-1} \overline{H}_1^T Y_{mea}^{set1} \tag{23}$$

$$Y_{rec}^{set2} = \overline{H}_2 F = \overline{H}_2 \left(\overline{H}_1^T \overline{H}_1 + \lambda I\right)^{-1} \overline{H}_1^T Y_{mea}^{set1} \tag{24}$$

where transmissibility matrix is $T_{12} = \overline{H}_2 (\overline{H}_1^T \overline{H}_1 + \lambda I)^{-1} \overline{H}_1^T$; λ is a non-negative regularization parameter. If $\lambda = 0$, equation (24) is transformed into the ordinary least squares solution $Y_{rec}^{set2} = \overline{H}_2 (\overline{H}_1^T \overline{H}_1)^{-1} \overline{H}_1^T Y_{mea}^{set1}$.

The key point is how to properly determine the regularization parameters λ. Compared with traditional L-curve method or generalized cross-validation method, As reported in the research (Feng et al., 2015), Bayesian inference regularization has higher computational efficiency, especially in solving problem with a large data set. Thus, statistical Bayesian inference approach is adopted in this study to obtain regularization parameter.

Angular displacement/acceleration recovery method

It is well-known that angular displacement and angular acceleration are more sensitive to the elemental stiffness reduction than translational measurements but they are difficult or expense to be accurately measured to some extent. In this section, according to the derived strain-to-displacement relationship in Reich and Park (2001), angular displacement/acceleration recovery method is developed to calculate the angular displacement/acceleration with translational displacement/acceleration and strain, respectively.

The displacement u of a beam element consists of rigid-body motion r and deformation d

$$u = d + r$$

The rigid-body motion r can be expressed as

$$r = \phi_\beta \beta \tag{25}$$

where ϕ_β stands for the elemental rigid-body modes; β denotes the rigid-body amplitudes.

According to the displacement-strain relation $\varepsilon = Su$, strain responses of a beam element can be written as following equation since strain would not be generated by rigid body motion $\phi_\beta \beta$

$$\varepsilon = Su = S(d + r) = Sd \tag{26}$$

By equation (26), deformation d can be derived as

$$d = \phi_\varepsilon \varepsilon = \left(S^T S\right)^{-1} S^T \varepsilon \tag{27}$$

The displacement u of a beam element can be further expressed as

$$u = d + r = \phi_\varepsilon \varepsilon + \phi_\beta \beta \tag{28}$$

In equation (28), $\phi_\varepsilon \varepsilon$ and $\phi_\beta \beta$ stand for deformation and rigid-body motion, respectively. For a beam element, displacements u consists of translational displacement u_w and angular displacement u_θ, so equation (28) is divided into translation and rotation as follows

$$\begin{bmatrix} u_w \\ u_\theta \end{bmatrix} = \begin{bmatrix} \phi_{\varepsilon w} \\ \phi_{\varepsilon\theta} \end{bmatrix} \varepsilon + \begin{bmatrix} \phi_{\beta w} \\ \phi_{\beta\theta} \end{bmatrix} \beta \tag{29}$$

where translational displacement and angular displacement are $u_w = [\,u_{w_1} \quad u_{w_2}\,]^T$ and $u_\theta = [\,u_{\theta_1} \quad u_{\theta_2}\,]^T$ for two nodes of a beam element.

In general, translational displacements u_w and elemental strains ε can be directly measured using various sensors, such as computer vision-based displacement sensors and long-gauge fiber Bragg grating (LFBG) strain sensors, conveniently. Accordingly, an angular displacement recovery method is used to acquire the unknown angular displacement u_θ with translational displacements u_w and strains ε measured from the same element. Rigid-body amplitudes β and angular displacement u_θ can be easily derived from equation (29) as

$$\begin{bmatrix} \beta \\ u_\theta \end{bmatrix} = \begin{bmatrix} -\phi_{\beta w} & 0 \\ -\phi_{\beta\theta} & I \end{bmatrix}^{-1} \left\{ \begin{bmatrix} \phi_{\varepsilon w} \\ \phi_{\varepsilon\theta} \end{bmatrix} \varepsilon - \begin{bmatrix} I \\ 0 \end{bmatrix} u_w \right\} \tag{30}$$

Compared with displacements and strains, acceleration responses contain more global response features and are widely used in structural health monitoring system. In order to compute the angular acceleration $\ddot{u}_\theta$, an angular acceleration recovery method is developed from the equation (30) as follows

$$\begin{bmatrix} \ddot{\beta} \\ \ddot{u}_\theta \end{bmatrix} = \begin{bmatrix} -\phi_{\beta w} & 0 \\ -\phi_{\beta\theta} & I \end{bmatrix}^{-1} \left\{ \begin{bmatrix} \phi_{\varepsilon w} \\ \phi_{\varepsilon\theta} \end{bmatrix} \ddot{\varepsilon} - \begin{bmatrix} I \\ 0 \end{bmatrix} \ddot{u}_w \right\} \tag{31}$$

where $\ddot{\varepsilon}$ means the second-order derivative of strain measurements; $\ddot{u}_w$ represents translational accelerations and they can be directly measured by accelerometers.

It is clear in the proposed angular acceleration recovery method, $\ddot{\varepsilon}$ is required. To calculate the second-order derivative of strain measurements, selecting a favorable differentiation method is important since improper methods would amplify the noise effect in the high order derivative calculation. In previous studies, some derivative calculation methods have been reported, such as conventional numerical differentiation, Fourier transform, Savitzky-Golay differentiation algorithm, discrete wavelet transform (DWT). In this work, continuous wavelet transform (CWT) method is adopted for derivative calculation in view of its merits over aforementioned methods, such as no requirement for the number of data points, simple operation, fast efficiency. The calculation of second derivative of strain signals is conducted by applying twice wavelet transform to the strain measurements.

The recovered angular displacement and recovered angular acceleration are obtained by using the proposed recovery method. Subsequently, they are used to establish the objective function.

Damage identification model

Proposed objective function

Generally, the structural local damage is considered as the linear reduction of structural stiffness and the damage effect on the mass is directly neglected (Law et al., 2011; Li and Hao, 2014; Zhang and Xu, 2017). A series of elemental stiffness reduction vectors $\alpha = (\alpha_1, \alpha_2, ..., \alpha_i, ...\alpha_{ne})$ are introduced to describe the local damage model as follows

$$K_{da} = \sum_{i=1}^{ne} (1 - \alpha_i) K_i^e, 0 \le \alpha_i \le 1 \tag{32}$$

where K_{da} and K_i^e stand for the stiffness matrix in the damaged state and the i-th elemental stiffness matrix in the intact status, respectively; ne denotes the number of elements; α_i is the stiffness reduction extent of the i-th element ranging from 0 to 1. $\alpha_i = 1$ indicates the i-th element is totally damaged, and $\alpha_i = 0$ means this element is intact. Structural stiffness vector to be identified are $\theta_i = (1 - \alpha_i), i = 1, 2, ..., ne$.

Substructural damage identification can be transformed into an optimization-based inverse problem. A suitable objective function needs to be defined, which is optimized to determine the optimal stiffness parameters. The traditional objective function, denoted as $Obj1$, is constructed based on the measured acceleration responses $\ddot{u}_{mea}^{set2}$ and the reconstructed acceleration responses $\ddot{u}_{rec}^{set2}$ of measurement set 2 from the target substructure in the damaged state as follows

$$Obj1 = \frac{\left\| \ddot{u}_{mea}^{set2} - \ddot{u}_{rec}^{set2}(\theta) \right\|_2}{\left\| \ddot{u}_{mea}^{set2} \right\|_2} \tag{33}$$

where $\ddot{u}_{mea}^{set2}$ is directly measured from the substructure; $\ddot{u}_{rec}^{set2}(\theta)$ is reconstructed using response reconstruction technique.

When multiple types of sensors are installed on the substructure, heterogeneous measurements (displacement, strain, acceleration) would be obtained. The second objective function based on rescaled heterogeneous measurements Y, denoted as $Obj2$, is constructed as

$$Obj2 = \frac{\left\| Y_{mea}^{set2} - Y_{rec}^{set2}(\theta) \right\|_2}{\left\| Y_{mea}^{set2} \right\|_2} \tag{34}$$

where Y_{mea}^{set2} means the heterogeneous data of set 2 directly measured from the target substructure; $Y_{rec}^{set2}(\theta)$ is the reconstructed heterogeneous data of measurement set 2 using the proposed heterogeneous response reconstruction technique.

In addition, a new objective function, denoted as $Obj3$, is proposed based on the recovered angular displacement u_θ and recovered angular acceleration $\ddot{u}_\theta$ of measurement set 2 as follows

$$Obj3 = \frac{\left\| \ddot{Y}_{mea}^{set2} - \ddot{Y}_{rec}^{set2}(\theta) \right\|_2}{\left\| \ddot{Y}_{mea}^{set2} \right\|_2} \tag{35}$$

where $\ddot{Y}_{mea}^{set2}$ represents the recovered angular displacement and angular acceleration using measured heterogeneous data of set 2, $\ddot{Y}_{mea}^{set2} = \left[u_{\theta,mea}^{set2} \quad \ddot{u}_{\theta,mea}^{set2} \right]^T$; $\ddot{Y}_{rec}^{set2}(\theta)$ implies the recovered angular displacement and angular acceleration using reconstructed heterogeneous data of set 2, $\ddot{Y}_{rec}^{set2} = \left[u_{\theta,rec}^{set2} \quad \ddot{u}_{\theta,rec}^{set2} \right]^T$.

The heterogeneous responses are initially measured from the selected substructure with multi-type sensors and then divided into set 1 Y_{mea}^{set1} and set 2 Y_{mea}^{set2}. Next, the measured responses of set 1 Y_{mea}^{set1} are used to reconstruct the responses of measurement set 2 Y_{rec}^{set2}. Subsequently, for the responses in Y_{mea}^{set2} and Y_{rec}^{set2}, translational displacements and strains are utilized to compute the angular displacements, meanwhile translational accelerations and strain are used to calculate the angular accelerations. In this way, recovered signals $\ddot{Y}_{mea}^{set2}$ and $\ddot{Y}_{rec}^{set2}$ are obtained. Finally, the objective function for damage identification *Obj*3 is established based on the recovered signals of measured and reconstructed response set 2. The performance of these three objective functions will be compared in numerical study. Besides, to further indicate the superiority of the proposed objective function.

Q-learning hybrid evolutionary algorithm

Evolutionary algorithms have been employed to damage identification and model updating because they have advantages of easy operation, good robustness, loose requirement on initial condition. A related review was given in Ref. (Alkayem et al., 2018). An emerging heuristic algorithm, named Jaya algorithm, has been developed and widely used to solve diverse engineering problems. Compared with GA, PSO, grey wolf optimizer, butterfly optimization algorithm, Jaya algorithm has simpler structure and it does not require any algorithm-specific parameters. In the basic Jaya algorithm, the feasible solutions would move toward the best solution meanwhile escape from the worst solution. In other words, only the best and worst solutions are involved in the generation of new feasible solutions. It is difficult to achieve the tradeoff between exploration and exploitation with the relatively single and monotonous local search operation. In this regard, some modifications need to be conducted to improve the performance of Jaya algorithm. DE algorithm is an effective global optimization algorithm dealing with complex optimization problems considering its multiple search strategies, such as DE/rand/1, DE/best/1, DE/rand/2, DE/best/2, DE/current-to-best/1, DE/rand-to-best/1. Inspired the idea that different search strategies have their own advantages and disadvantages, a search strategy pool is proposed by combining four search strategies i.e., DE/rand/1, DE/rand/2, DE/current-to-best/1 and Jaya mutation as follows

$$Strategy\,pool = \begin{cases} Group_1 \begin{cases} DE/rand/1 \\ DE/rand/2 \end{cases} \\ Group_2 \begin{cases} DE/current-to-best/1 \\ Jaya\ mutation \end{cases} \end{cases} \tag{36}$$

where $Group_1$ concentrates on exploration mode, composed of DE/rand/1 and DE/rand/2; $Group_2$ focuses on exploitation mode, containing DE/current-to-best/1 and Jaya mutation.

The updating equation of the proposed strategy pool can be expressed as

$$Strategy\,pool = \begin{cases} V_{i,G} = X_{r_1,G} + F_m(X_{r_2,G} - X_{r_3,G}) \\ V_{i,G} = X_{r_1,G} + F_m(X_{r_2,G} - X_{r_3,G}) \\ \qquad + F_m(X_{r_4,G} - X_{r_5,G}) \\ V_{i,G} = X_{i,G} + F_m(X_{best,G} - X_{i,G}) \\ \qquad + F_m(X_{r_1,G} - X_{r_2,G}) \\ V_{i,j,G} = X_{i,j,G} + rand_1 \\ \qquad \times \left(X_{best,j,G} - \left|X_{i,j,G}\right|\right) - rand_2 \\ \qquad \times \left(X_{worst,j,G} - \left|X_{i,j,G}\right|\right) \end{cases} \tag{37}$$

where subscripts r_1, r_2, r_3, r_4, r_5 are randomly selected from the current population; F_m stands for the mutation parameter taken from the range of [0, 1]; $rand_1$ and $rand_2$ are two uniformly random numbers in [0, 1]; $X_{best,j,G}$ and $X_{worst,j,G}$ represent the best and worst individuals of the j-th variable in the G-th iteration, respectively.

To adaptively select the best operation from the search strategy pool for each individual within the population, a popular reinforced learning algorithm, Q-learning, is adopted in this study, which has a valid idea that the agent will take the optimal action for the alternation of state and accordingly it receives immediate rewards or punishments. Agent, environment, states, actions, and rewards are five essential components of Q-learning algorithm. During the iteration process, rewards or punishments after conducting each given action are analyzed for every agent. The action with the maximum reward (Q-value) would be opted. The action act_t in the given state sta_t is evaluated using Bellman equation as (Cao et al., 2023).

$$\begin{aligned} Q^{new}(sta_t, act_t) = Q(sta_t, act_t) + \varphi[rew_{t+1} + \\ \eta \cdot \max Q(sta_{t+1}, act_t) - Q(sta_t, act_t)] \end{aligned} \tag{38}$$

where $Q^{new}(sta_t, act_t)$ and $Q(sta_t, act_t)$ stand for the updated and previous Q-values; φ represents the learning rate;

rew_{t+1} denotes the received immediate rewards; η means the discount factor; $\max Q(sta_{t+1}, act_t)$ is the maximum Q-value for all actions. As suggested in Ref. (Kaveh et al., 2022), discount factor $\eta = 0.8$ and learning rate $\varphi(Iter) = 1 - 0.9 \times \frac{Iter}{Max\_Iter}$ are set, in which *Iter* and *Max_Iter* are current and maximum iteration number, respectively.

Integrating Jaya algorithm, DE, Q-learning algorithm, Q-learning hybrid evolutionary algorithm is proposed. When solving structural/substructural parameter identification problem using the proposed QHEA, some analogies with Q-learning framework should be given. The individuals in the population are the candidate stiffness vectors to be identified, which are viewed as the learning agents; the environment is regarded as the search domain of these candidate stiffness vectors; the states refer to the possible operations from strategy pool, i.e., DE/rand/1, DE/rand/2, DE/current-to-best/1 and Jaya mutation for candidate solutions; the action implies it switches from one updating strategy to another.

For individuals in each iteration, the most suitable search operation is selected adaptively and continuously from the strategy pool, for the proposed QHEA, under the guidance of the Q-learning based on the maximum Q-value in the Q-table.

Procedures of the proposed approach

The procedures of the proposed output-only damage identification approach are further described as follows:

Step 1: predefine the algorithm parameters and generate the initial guess of structural parameters within the search domain, establishing the digital twin virtual model corresponding to physical structure.

Step 2: in dynamic response reconstruction model, obtain heterogeneous responses (displacements, strains, accelerations, etc.,) from the target substructure with preinstalled multi-type sensors (displacement transducers, strain gauges, accelerometers, etc.,) and then divide them into two measurement sets, i.e., measured responses of set 1 Y_{mea}^{set1} and measured responses of set 2 Y_{mea}^{set2}.

Step 3: calculate the unit impulse response function under external and internal forces, and then assemble the rescaled unit impulse response matrices H_1 and H_2 with equations (13a), (13b), (13c), (14a), (14b), (14c), and (16).

Step 4: determine regularization parameter λ with Bayesian inference regularization and reconstruct responses of measurement set 2 Y_{rec}^{set2} from the finite element model with the measured responses of set 1 Y_{mea}^{set1}.

Step 5: calculate the recovered angular acceleration and recovered angular displacement for Y_{mea}^{set2} and Y_{rec}^{set2} using the proposed recovery method.

Step 6: in damage identification model, compute objective function *Obj*3 based on the recovered signals of measured and reconstructed response set 2, i.e., $\ddot{Y}_{mea}^{set2}$ and $\ddot{Y}_{rec}^{set2}$, updating substructural parameters with the proposed QHEA.

Step 7: repeat steps 3-6 until the maximum iteration reached or the convergence criterion satisfied.

Step 8: output the final detected damage locations and extents of the target substructure.

Numerical studies

To validate the performance of the proposed output-only damage identification method, the three-span beam structure as shown in Figure 2(a) is employed as an example. The total length and cross-sectional area of the beam structure are 4000 mm and 50 mm × 6 mm. It is discretized into 40 Euler- Bernoulli beam elements, so the length of each element is 100 mm. The beam structure has 41 nodes, 80 DOFs, a hinge support at the node 11 and a roller support at the node 31. The Young's modulus and mass density for the used steel material are 2.1×10^{11} N/m^2 and 7860 kg/m^3, respectively. Two random input excitations are vertically applied at nodes 23 and 36, respectively. It is observed from Figure 2(a), the whole structure is divided into two substructures, substructure *a* on the left side and substructure *b* on the right side. The substructure *a* contains elements 1-18 and substructure *b* includes elements 19-40. There are shear force and bending moment from adjacent substructures.

The substructure *a* is taken as the example to derive the proposed recovery method. As shown in Figure 2(b), the nodal displacements of element 4 or element 9 are $u = [u_{w_1} \quad u_{\theta_1} \quad u_{w_2} \quad u_{\theta_2}]^T$ and the bending strains at two Barlow points are $\varepsilon_1\left(-\frac{1}{\sqrt{3}}, \frac{y}{2}\right)$ and $\varepsilon_2\left(\frac{1}{\sqrt{3}}, \frac{y}{2}\right)$. Thus, the strain-displacement relation of a beam element can be expressed as

$$\begin{bmatrix} \varepsilon_1\left(-\frac{1}{\sqrt{3}}, \frac{y}{2}\right) \\ \varepsilon_2\left(\frac{1}{\sqrt{3}}, \frac{y}{2}\right) \end{bmatrix} = -\frac{y}{L^2}\begin{bmatrix} -\sqrt{3} & -\frac{(1+\sqrt{3})L}{2} & \sqrt{3} & \frac{(1-\sqrt{3})L}{2} \\ \sqrt{3} & -\frac{(1-\sqrt{3})L}{2} & -\sqrt{3} & \frac{(1+\sqrt{3})L}{2} \end{bmatrix} \times \begin{bmatrix} u_{w_1} \\ u_{\theta_1} \\ u_{w_2} \\ u_{\theta_2} \end{bmatrix} \tag{39}$$

where y and L denote the thickness and length of beam element.

ϕ_ε and ϕ_β in equation (28) are

$$\phi_\varepsilon = \frac{L}{6y\left(L^2+4\right)} \begin{bmatrix} 2\sqrt{3}L & -2\sqrt{3}L \\ 12+\left(3+\sqrt{3}\right)L^2 & 12-\left(-3+\sqrt{3}\right)L^2 \\ -2\sqrt{3}L & 2\sqrt{3}L \\ -12+\left(-3+\sqrt{3}\right)L^2 & -12-\left(3+\sqrt{3}\right)L^2 \end{bmatrix},$$

$$\phi_\beta = \begin{bmatrix} 1 & -L \\ 0 & 2 \\ 1 & L \\ 0 & 2 \end{bmatrix} \tag{40}$$

The nodal displacements of element 9 can be written as

$$\begin{bmatrix} u_{w_1} \\ u_{\theta_1} \\ u_{w_2} \\ u_{\theta_2} \end{bmatrix} = \frac{L}{6y\left(L^2+4\right)} \begin{bmatrix} 2\sqrt{3}L & -2\sqrt{3}L \\ 12+\left(3+\sqrt{3}\right)L^2 & 12-\left(-3+\sqrt{3}\right)L^2 \\ -2\sqrt{3}L & 2\sqrt{3}L \\ -12+\left(-3+\sqrt{3}\right)L^2 & -12-\left(3+\sqrt{3}\right)L^2 \end{bmatrix} \begin{bmatrix} \varepsilon_1\left(-\frac{1}{\sqrt{3}},\frac{y}{2}\right) \\ \varepsilon_2\left(\frac{1}{\sqrt{3}},\frac{y}{2}\right) \end{bmatrix} + \begin{bmatrix} 1 & -L \\ 0 & 2 \\ 1 & L \\ 0 & 2 \end{bmatrix} \begin{bmatrix} \beta_1 \\ \beta_2 \end{bmatrix} \tag{41}$$

From equation (30), angular displacements (u_{θ_1} and u_{θ_2}) of element 4 and element 9 can be easily recovered with translational displacements (u_{w_1} and u_{w_2}) and strains (ε_1 and ε_2) as

$$\begin{bmatrix} \beta_1 \\ \beta_2 \\ u_{\theta_1} \\ u_{\theta_2} \end{bmatrix} = \begin{bmatrix} -1 & L & 0 & 0 \\ -1 & -L & 0 & 0 \\ 0 & -2 & 1 & 0 \\ 0 & -2 & 0 & 1 \end{bmatrix}^{-1} \left\{ \frac{L}{6y\left(L^2+4\right)} \begin{bmatrix} 2\sqrt{3}L & -2\sqrt{3}L \\ -2\sqrt{3}L & 2\sqrt{3}L \\ 12+\left(3+\sqrt{3}\right)L^2 & 12-\left(-3+\sqrt{3}\right)L^2 \\ -12+\left(-3+\sqrt{3}\right)L^2 & -12-\left(3+\sqrt{3}\right)L^2 \end{bmatrix} \times \begin{bmatrix} \varepsilon_1\left(-\frac{1}{\sqrt{3}},\frac{y}{2}\right) \\ \varepsilon_2\left(\frac{1}{\sqrt{3}},\frac{y}{2}\right) \end{bmatrix} - \begin{bmatrix} 1 & 0 \\ 0 & 1 \\ 0 & 0 \\ 0 & 0 \end{bmatrix} \begin{bmatrix} u_{w_1} \\ u_{w_2} \end{bmatrix} \right\} \tag{42}$$

From equation (31), angular accelerations ($\ddot{u}_{\theta_1}$ and $\ddot{u}_{\theta_2}$) of element 13 and element 16 can be calculated with translational accelerations ($\ddot{u}_{w_1}$ and $\ddot{u}_{w_2}$) and the second-order derivative of strains ($\ddot{\varepsilon}_1$ and $\ddot{\varepsilon}_2$)

$$\begin{bmatrix} \ddot{\beta}_1 \\ \ddot{\beta}_2 \\ \ddot{u}_{\theta_1} \\ \ddot{u}_{\theta_2} \end{bmatrix} = \begin{bmatrix} -1 & L & 0 & 0 \\ -1 & -L & 0 & 0 \\ 0 & -2 & 1 & 0 \\ 0 & -2 & 0 & 1 \end{bmatrix}^{-1} \left\{ \frac{L}{6y(L^2+4)} \begin{bmatrix} 2\sqrt{3}L & -2\sqrt{3}L \\ -2\sqrt{3}L & 2\sqrt{3}L \\ 12+\left(3+\sqrt{3}\right)L^2 & 12-\left(-3+\sqrt{3}\right)L^2 \\ -12+\left(-3+\sqrt{3}\right)L^2 & -12-\left(3+\sqrt{3}\right)L^2 \end{bmatrix} \times \begin{bmatrix} \ddot{\varepsilon}_1\left(-\frac{1}{\sqrt{3}}, \frac{y}{2}\right) \\ \ddot{\varepsilon}_2\left(\frac{1}{\sqrt{3}}, \frac{y}{2}\right) \end{bmatrix} - \begin{bmatrix} 1 & 0 \\ 0 & 1 \\ 0 & 0 \\ 0 & 0 \end{bmatrix} \begin{bmatrix} \ddot{u}_{w_1} \\ \ddot{u}_{w_2} \end{bmatrix} \right\} \tag{43}$$

Substructure a

For substructure a, there are four displacement sensors, eight strain sensors, six accelerometers installed, as presented in Figure 2(b). Nodal displacements and nodal accelerations in vertical direction as well as flexural deformations of beam element are measured. These measurements are divided into two sets. Measurement set 1 includes eight heterogeneous measurements, including two displacement responses (from nodes 9 and 10), four strain responses (from elements 9 and 16), two acceleration responses (from nodes 16 and 17). Measurement set 2 contains ten heterogeneous measurements, including two displacement responses (from nodes 4 and 5), four strain responses (from elements 4 and 13), four acceleration responses (from nodes 2, 8, 13 and 14). Two interface forces act at node 19. Obviously, the number of measurements in the set 1 is larger than the number of interface forces. The sampling duration is set as 1 s with the sampling frequency of 1000 Hz. White Gaussian noise is added into the calculated dynamic responses to simulate the effect of measurement noise. Three different levels of noise, i.e., 0%, 5% and 10%, are considered in this numerical study, $noise = Nl \times N_{noise} RMS(Y)$.

Response reconstruction for substructure a. The responses at the sensor location for the measurement set 2 are reconstructed with the measured responses in the set 1 when the structural parameters are known. Then, the reconstructed responses are compared with the measured values. The relative error (*RE*) and Pearson correlation coefficient (*PCC*) are utilized to evaluate the accuracy of response reconstruction as follows

$$RE = \frac{\|Y_{rec} - Y_{mea}\|_2}{\|Y_{mea}\|_2} \times 100\% \tag{44}$$

$$PCC(Y_{mea}, Y_{rec}) = \frac{Cov(Y_{mea}, Y_{rec})}{\sigma_{Y_{mea}} \sigma_{Y_{rec}}} \tag{45}$$

where Y_{mea} and Y_{rec} represent the measured and reconstructed heterogeneous data, respectively; $\sigma_{Y_{mea}}$ and $\sigma_{Y_{rec}}$ stand for the standard deviation of Y_{mea} and Y_{rec}.

After implementing heterogeneous response reconstruction and recovery method, recovered angular displacements and angular accelerations are obtained. Figures 3 and 4 present the recovered angular displacement at node 4 and the recovered angular acceleration at node 13, respectively. It can be easily observed that the measured responses almost overlap with reconstructed values without and with noise. By Figures 3(b) and 4(b), the discrepancy amplitudes are 10^{-15} and 10^{-12} for noise free case. The relative errors and Pearson correlation coefficients between reconstructed and measured responses of measurement set 2 are listed in Table 1. The maximum relative errors among these responses are 6.58% and 13.06% for 5% and 10% noise case, respectively, which implies a favorable accuracy of response reconstruction is achieved.

Damage identification results for substructure a. The proposed substructural damage identification approach is investigated. For substructure a, there are 18 elements involved in the inverse analysis. It is assumed that there are 15% and 5%

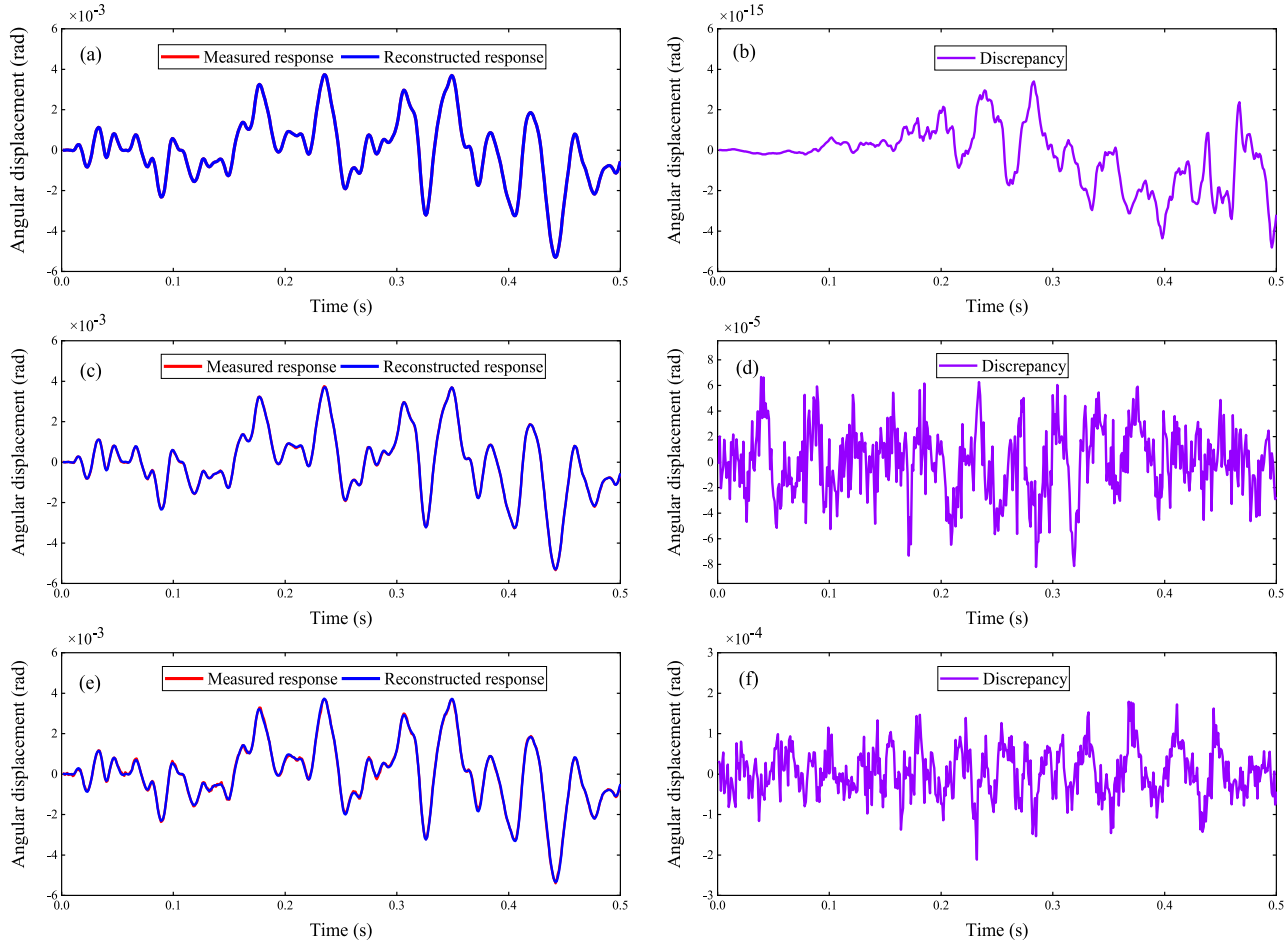

Figure 3. The recovered angular displacement at node 4: (a) comparison without noise; (b) discrepancy without noise; (c) comparison with 5% noise; (d) discrepancy with 5% noise; (e) comparison with 10% noise; (f) discrepancy with 10% noise.

stiffness reductions at elements 6 and 15, namely, $\alpha_6 = 0.15$, $\alpha_{15} = 0.05$. The measured and reconstructed acceleration responses of measurement set 2 (from nodes 2, 8, 13 and 14) are used to established the first objective function *Obj*1. The measured and reconstructed heterogeneous responses of measurement set 2 are used to established the second objective function *Obj*2. The recovered angular displacements (from nodes 4 and 5), recovered angular accelerations (from nodes 13 and 14) are used to established the third objective function *Obj*3. QHEA is used as search tool to optimize these three objective functions. The parameters of QHEA are set as: population size $NP = 60$, maximum iterations $Max\_Iter = 200$, mutation parameter $F = 0.8$, discount factor $\gamma = 0.8$. The identified damage results using objective functions *Obj*1, *Obj*2, *Obj*3 under 0%, 5%, 10% noises are presented in Figure 5.

For the noise-free case, the identified damage extents at elements 6 and 15 are 13.19% and 4.62% using *Obj*1, which slightly deviates from the accurate values but still acceptable from practical point of view. When contaminated with 5% noise, however, some large false identifications are apparently observed at the 1st, 15th, 18th elements. The damaged element 15 is even recognized as a health element for the case with 10% noise, which implies 5% small stiffness reduction is difficult to be accurately detected when high noise-polluted acceleration responses are utilized alone. In contrast, it can be found from Figure 5(a) that pleasant identification results are acquired using *Obj*2 and *Obj*3 with maximum errors of 1.40% and 0.33% and mean errors of 0.29% and 0.02%, respectively. In Figure 5(b) and (c), the identified damage extents are quite close to the exact values when the measurements are contaminated by 5% and 10% noise. Compared with *Obj*2, less false identifications are observed by using *Obj*3, which verifies its advantages in terms of accuracy of damage detection owing to recovered angular displacements and angular accelerations involved in objective function. The main reason is that angular displacements and angular accelerations are more sensitive to substructural element stiffness than translational responses.

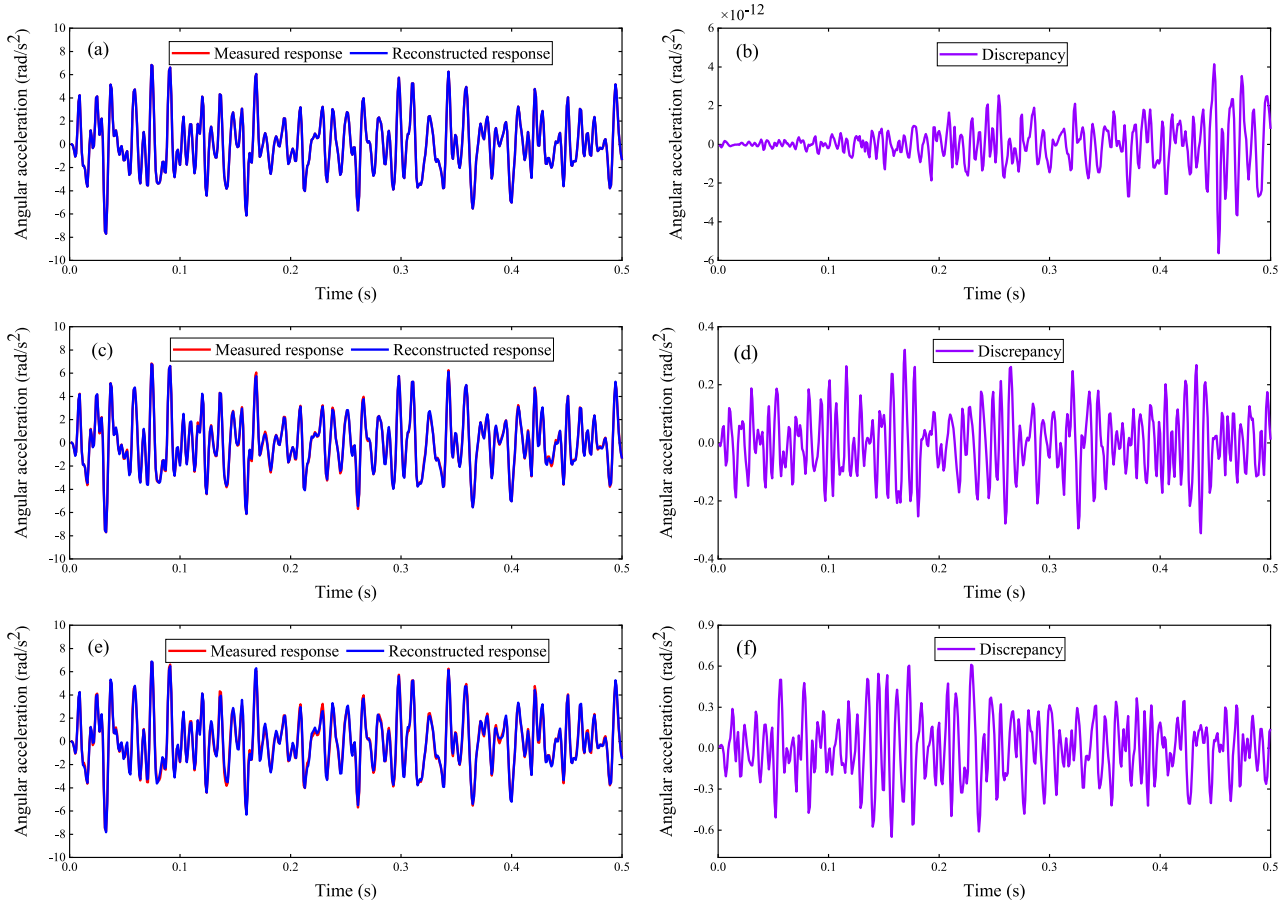

Figure 4. The recovered angular acceleration at node 13: (a) comparison without noise; (b) discrepancy without noise; (c) comparison with 5% noise; (d) discrepancy with 5% noise; (e) comparison with 10% noise; (f) discrepancy with 10% noise.

Table 1. Relative errors and Pearson correlation coefficients between reconstructed and measured responses for substructure *a*.

	0% noise		5% noise		10% noise	
Type of reconstruction	*RE* (%)	*PCC*	*RE* (%)	*PCC*	*RE* (%)	*PCC*
Translational displacements at node 4	1.95×10^{-11}	1.00	4.90	0.9988	9.72	0.9952
Translational displacements at node 5	1.99×10^{-11}	1.00	5.21	0.9986	9.74	0.9952
Left strain response at element 4	1.00×10^{-10}	1.00	5.50	0.9985	10.23	0.9948
Right strain response at element 4	1.01×10^{-10}	1.00	5.04	0.9987	9.95	0.9950
Left strain response at element 13	4.87×10^{-11}	1.00	4.76	0.9989	10.01	0.9950
Right strain response at element 13	4.86×10^{-11}	1.00	5.08	0.9987	10.22	0.9948
Translational acceleration at node 2	7.19×10^{-10}	1.00	5.35	0.9986	10.71	0.9943
Translational acceleration at node 8	3.10×10^{-10}	1.00	5.78	0.9983	11.58	0.9934
Translational acceleration at node 13	1.28×10^{-10}	1.00	6.58	0.9979	13.06	0.9914
Translational acceleration at node 14	1.30×10^{-10}	1.00	6.53	0.9979	12.84	0.9917
Recovered angular displacement at node 4	9.27×10^{-11}	1.00	2.04	0.9998	3.00	0.9996
Recovered angular displacement at node 5	1.04×10^{-10}	1.00	2.14	0.9998	3.43	0.9994
Recovered angular acceleration at node 13	1.88×10^{-9}	1.00	4.57	0.9990	9.54	0.9954
Recovered angular acceleration at node 14	1.94×10^{-9}	1.00	4.65	0.9989	9.46	0.9956

Figure 6 shows the identification process of damage extents for noise-free case. The identified damage extents of the 6th and 15th elements sightly deviates from the exact solution to some extent using *Obj*1. It converges to the exact values for the proposed *Obj*2 and *Obj*3, around 70 and 20 iterations required, respectively, which demonstrates the superior performance of *Obj*3 in computational efficiency.

Substructure b

For substructure *b*, the sensor placement configuration is presented in Figure 2(c). There are four displacement sensors, eight strain sensors, eight accelerometers installed. The vertical nodal displacements and accelerations as well as flexural deformations of beam element are measured. These measurements are divided into two sets according to the heterogeneous response reconstruction theory. Measurement set 1 consists of ten heterogeneous measurements, including two displacement responses (from nodes 27 and 28), four strain responses (from elements 27 and 37), four acceleration responses (from nodes 20, 24, 37 and 38). Measurement set 2 contains ten heterogeneous measurements, including two displacement responses (from nodes 21 and 22), four strain responses (from elements

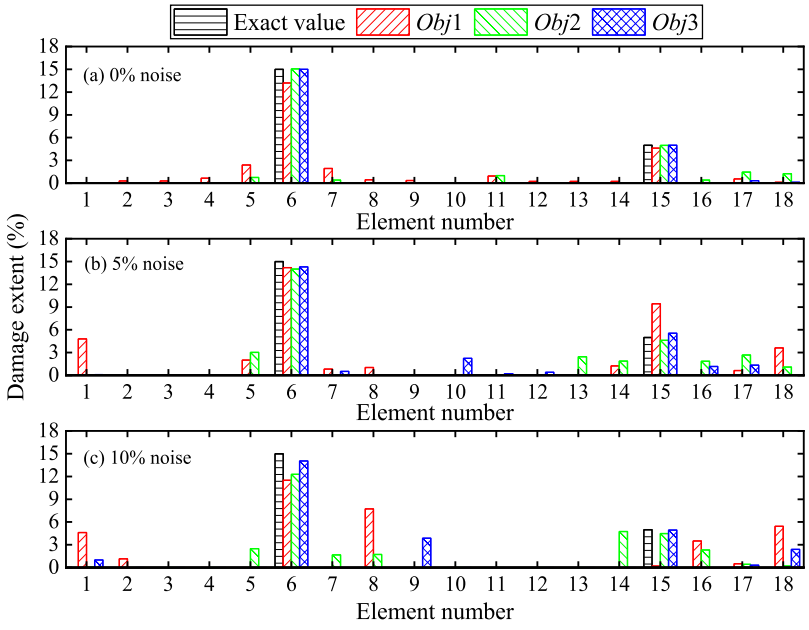

Figure 5. The identified results with three different objective function: (a) *Obj*1; (b) *Obj*2; (c) *Obj*3.

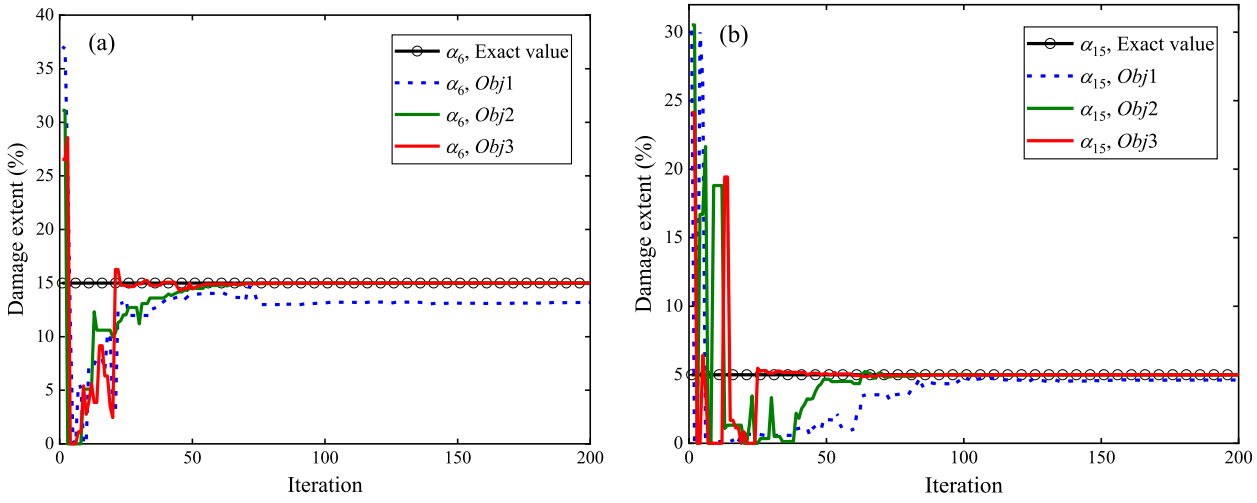

Figure 6. Identification process of damage extents for 0% noise case: (a) element 6; (b) element 15.

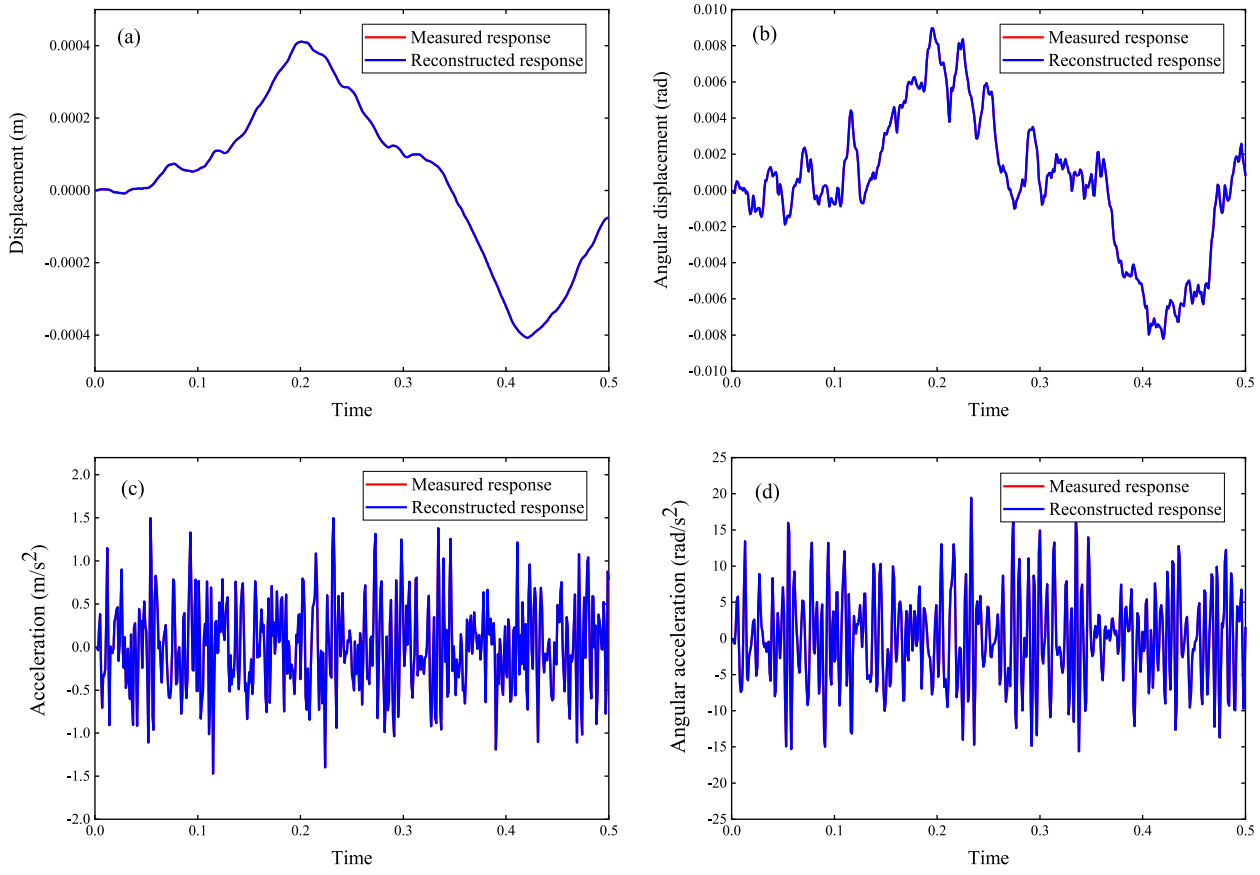

Figure 7. Comparison of the measured and reconstructed responses: (a) Displacement at node 21; (b) angular displacement at node 21; (c) acceleration at node 32; (d) angular acceleration at node 32.

Table 2. Relative errors and Pearson correlation coefficients between reconstructed and measured responses for substructure *b*.

	0% noise		5% noise		10% noise	
Type of reconstruction	*RE* (%)	*PCC*	*RE* (%)	*PCC*	*RE* (%)	*PCC*
Translational displacements at node 21	1.90×10^{-9}	1.00	4.34	0.9986	10.58	0.9947
Translational displacements at node 22	3.12×10^{-10}	1.00	4.15	0.9987	9.88	0.9950
Left strain response at element 21	3.59×10^{-8}	1.00	6.15	0.9979	10.70	0.9943
Right strain response at element 21	3.64×10^{-8}	1.00	6.82	0.9975	10.22	0.9948
Left strain response at element 32	4.11×10^{-10}	1.00	6.32	0.9978	10.31	0.9947
Right strain response at element 32	4.11×10^{-10}	1.00	6.01	0.9980	10.35	0.9947
Translational acceleration at node 26	2.52×10^{-8}	1.00	5.86	0.9982	10.19	0.9948
Translational acceleration at node 30	1.08×10^{-8}	1.00	5.82	0.9982	10.62	0.9942
Translational acceleration at node 32	4.68×10^{-10}	1.00	5.33	0.9985	10.85	0.9940
Translational acceleration at node 33	2.08×10^{-10}	1.00	5.38	0.9985	10.76	0.9943
Recovered angular displacement at node 21	3.99×10^{-8}	1.00	3.66	0.9993	5.26	0.9986
Recovered angular displacement at node 22	3.29×10^{-8}	1.00	3.54	0.9994	5.51	0.9982
Recovered angular acceleration at node 32	1.24×10^{-9}	1.00	4.63	0.9988	9.47	0.9958
Recovered angular acceleration at node 33	1.16×10^{-9}	1.00	4.68	0.9987	9.52	0.9957

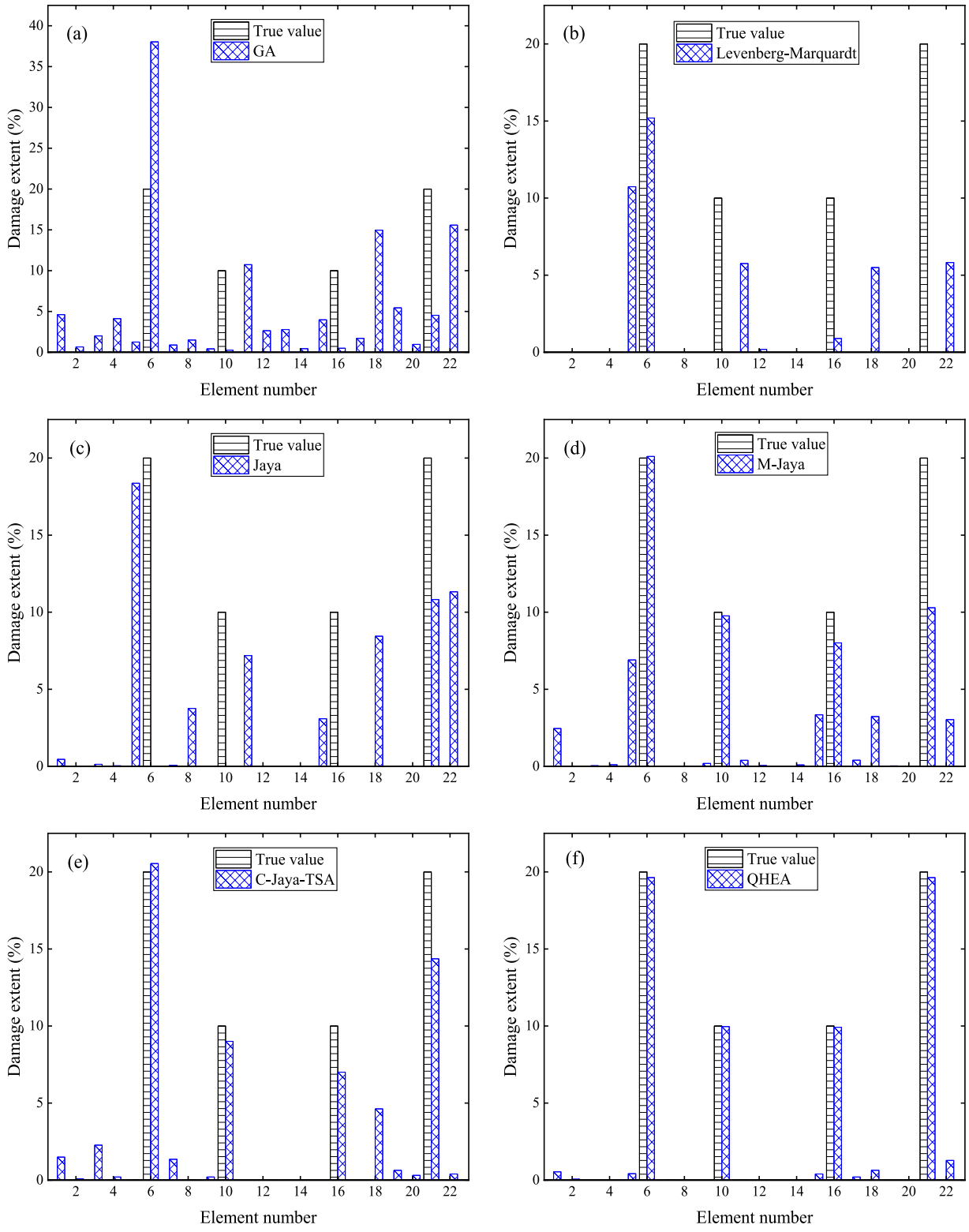

Figure 8. Identified results of substructure *b* using: (a) GA; (b) Levenberg-Marquardt method; (c) Jaya algorithm; M-Jaya; (d) C-Jaya-TSA; (f) QHEA.

Table 3. Identified extents for damaged element and relative errors with six different optimization methods

	Damage extent for element 24		Damage extent for element 28		Damage extent for element 34		Damage extent for element 39	
Algorithms	Identified	Error*	Identified	Error*	Identified	Error*	Identified	Error*
GA	38.03%	90.16%	0.27%	97.32%	0.49%	95.06%	4.53%	77.37%
LM	15.19%	24.04%	0%	100%	0.90%	91.03%	0%	100%
Jaya	0.02%	99.92%	0.02%	99.94%	0.015%	99.89%	10.82%	45.89%
M-Jaya	20.10%	0.49%	9.76%	2.40%	8.01%	19.91%	10.29%	48.55%
C-Jaya-TSA	20.54%	2.71%	9.00%	9.99%	7.01%	29.94%	14.36%	28.19%
QHEA	19.63%	1.85%	9.97%	0.34%	9.92%	0.79%	19.63%	1.86%
True value	20%	10%	10%	20%				

Note. Error* means the relative error.

21 and 32), four acceleration responses (from nodes 26, 30, 32 and 33). There are two external forces and two interface forces on the substructure, which are taken as unknown excitations. Obviously, the number of measurements in the set 1 is larger than the number of interface forces.

Response reconstruction for substructure b. To reveal the effectiveness of the dynamic response reconstruction model, Figure 7 presents the comparison of the measured and reconstructed responses, namely, displacement at node 21, angular displacement at node 21, acceleration at node 32, angular acceleration at node 32. It can be found that the reconstructed responses are extremely close to the measured ones. The amplitudes of angular displacement and angular acceleration are at least one order larger than those of the displacement at node 21 and acceleration at node 32. Besides, relative errors and Pearson correlation coefficients between reconstructed and measured responses for substructure b are listed in Table 2. The maximum relative errors among these responses are 3.99×10^{-8}, 6.82% and 10.85% for 0%, 5%, 10% noise cases, respectively, which denotes a good accuracy of response reconstruction is obtained.

Damage identification results for substructure b. For substructure b, there are 22 elements involved in the inverse analysis. Local damages are introduced as a reduction of stiffness in some specific elements. It is assumed that there are 20%, 10%, 10%, 20% stiffness reductions at the 24th, 28th, 34th and 39th elements, namely, $\alpha_{24} = 0.2$, $\alpha_{28} = 0.1$, $\alpha_{34} = 0.1$, $\alpha_{39} = 0.2$. The superior performance of the proposed $Obj3$ has been presented in the previous example, so only $Obj3$ is utilized in this section. The recovered angular displacements (from nodes 21 and 22), recovered angular accelerations (from nodes 32 and 33) are used to established the third objective function $Obj3$. The other five optimization techniques, including GA (Zhang et al., 2010), Levenberg-Marquardt (LM) method (Dkhichi et al., 2014), standard Jaya algorithm (Rao, 2016), M-Jaya (Zhang et al., 2023a, 2023b), hybrid C-Jaya-TSA (Ding et al., 2020) are compared with the proposed QHEA. The common parameters are set as population size $NP = 100$, maximum iterations $Max\_Iter = 200$. For GA, the mutation operator and crossover operator are 0.05 and 0.95. For Levenberg-Marquardt method, the initial values for all individuals are set as 0.8. For M-Jaya, the integer $\delta = 20$ and power exponent $v = 4$. For hybrid C-Jaya-TSA, the parameter ST is set as 0.4. The results of substructure b with these six optimization methods are shown in Figure 8 and Table 3.

As indicated in Figure 8(a)–(c) and Table 3, the traditional heuristic algorithm GA, classical LM algorithm and basic Jaya algorithm cannot correctly detect the locations and extents of multiple damages. M-Jaya and C-Jaya-TSA yield more accurate damage identification results but some large false identifications are still observed. In comparison with GA, Levenberg-Marquardt, standard Jaya algorithm, M-Jaya, C-Jaya-TSA, the proposed QHEA provide more satisfactory performance with less than 2% relative error for identified damaged elements.

Conclusions

In this paper, a digital twin framework for output-only substructural damage identification with data fusion of muti-type responses in time domain is proposed. A recovery method is developed to calculate the angular displacement with translational displacement and strain, the angular acceleration with translational acceleration and strain. In the damage identification model, a new objective function is formulated based on the recovered angular displacements and accelerations from the measured and reconstructed responses. Besides, a reinforced learning-assisted optimization algorithm QHEA is designed to solve the inverse problem until the convergence criteria is satisfied. Finally, the numerical studies are conducted to verify the capability and feasibility of the proposed method on

damage assessment. The following conclusions can be drawn:

(1) For translational displacements, strains, translational accelerations, angular displacements and angular accelerations, satisfactory response reconstruction results can be achieved with and without noise using heterogeneous response reconstruction technique and recovery method.
(2) Compared with *Obj*1 and *Obj*2, the proposed *Obj*3 demonstrates more superior performance in accuracy of damage detection and computational efficiency since angular displacement and angular acceleration are more sensitive to the alteration of elemental stiffness than translational displacement and translational acceleration.
(3) In comparison with GA, Levenberg-Marquardt, Jaya algorithm, M-Jaya, C-Jaya-TSA, the proposed QHEA could provide more favorable performance with less than 2% relative error for identified damaged elements because individuals could adaptively and continuously select the most suitable search strategy from the proposed strategy pool under the guidance of the Q-learning for QHEA.
(4) The results in the numerical studies show that the locations and extents of multiple damages can be accurately identified with the proposed output-only substructural damage identification approach, and the measurements at the interface DOFs are not required.

The key limitation of this work is that the force location is required, which is difficult to determine in some cases. In addition, the proposed method is only validated with numerical examples. In consideration of the good performance of the proposed digital twin framework for substruction damage identification, it can be extended to real structures in the future, such as bridges.

Declaration of conflicting interests

The author(s) declared no potential conflicts of interest with respect to the research, authorship, and/or publication of this article.

Funding

The author(s) disclosed receipt of the following financial support for the research, authorship, and/or publication of this article: the National Natural Science Foundation of China (52178115), the National Key R&D Program of China (2021YFE0112200), the Japan Society for Promotion of Science (Kakenhi No. 18K04438), the Japan Society for the Promotion of Science (Grant No. P23371), the Tohoku Institute of Technology Research Grant and the Postgraduate Research & Practice Innovation Program of Jiangsu Province (KYCX23_0273). Besides, the first author acknowledges China Scholarship Council (CSC 202306090271) to support study in the School of Civil and Mechanical Engineering at Curtin University.

ORCID iDs

Zhenwei Zhou https://orcid.org/0000-0002-1940-2697
Chunfeng Wan https://orcid.org/0000-0002-4236-6428

References

Ai L, Soltangharaei V and Ziehl P (2022) Developing a heterogeneous ensemble learning framework to evaluate Alkali-silica reaction damage in concrete using acoustic emission signals. *Mechanical Systems and Signal Processing* 172: 108981.

Ai L, Zhang B and Ziehl P (2023a) A transfer learning approach for acoustic emission zonal localization on steel plate-like structure using numerical simulation and unsupervised domain adaptation. *Mechanical Systems and Signal Processing* 192: 110216.

Ai L, Bayat M and Ziehl P (2023b) Localizing damage on stainless steel structures using acoustic emission signals and weighted ensemble regression-based convolutional neural network. *Measurement* 211: 112659.

Ai L, Soltangharaei V, Greer B, et al. (2024) Structural health monitoring of stainless-steel nuclear fuel storage canister using acoustic emission. *Developments in the Built Environment* 17: 100294.

Alkayem NF, Cao MS, Zhang YF, et al. (2018) Structural damage detection using finite element model updating with evolutionary algorithms: a survey. *Neural Computing & Applications* 30: 389–411.

Cao P, Zhang Y, Zhou K, et al. (2023) A reinforcement learning hyper-heuristic in multi-objective optimization with application to structural damage identification. *Structural and Multidisciplinary Optimization* 66(1): 16.

Ding ZH, Li J and Hao H (2019) Structural damage identification using improved Jaya algorithm based on sparse regularization and Bayesian inference. *Mechanical Systems and Signal Processing* 132: 211–231.

Ding ZH, Li J and Hao H (2020) Non-probabilistic method to consider uncertainties in structural damage identification based on Hybrid Jaya and Tree Seeds Algorithm. *Engineering Structures* 220: 110925.

Ding ZH, Hou RR and Xia Y (2022) Structural damage identification considering uncertainties based on a Jaya algorithm with a local pattern search strategy and L0. 5 sparse regularization. *Engineering Structures* 261: 114312.

Dkhichi F, Oukarfi B, Fakkar A, et al. (2014) Parameter identification of solar cell model using Levenberg–Marquardt algorithm combined with simulated annealing. *Solar Energy* 110: 781–788.

Doebling SW, Farrar CR and Prime MB (1998) A summary review of vibration-based damage identification methods. *The Shock and Vibration Digest* 30(2): 91–105.

T Elshazli M, Saras N and Ibrahim A (2022) Structural response of high strength concrete beams using fiber reinforced polymers under reversed cyclic loading. *Sustainable Structures* 2(2): 000018.

Feng DM, Sun H and Feng MQ (2015) Simultaneous identification of bridge structural parameters and vehicle loads. *Computers & Structures* 157: 76–88.

Feng K, González A and Casero M (2021) A kNN algorithm for locating and quantifying stiffness loss in a bridge from the forced vibration due to a truck crossing at low speed. *Mechanical Systems and Signal Processing* 154: 107599.

Hou J, Li Z, Zhang Q, et al. (2020) Local mass addition and data fusion for structural damage identification using approximate models. *International Journal of Structural Stability and Dynamics* 20(11): 2050124.

Jayalakshmi V, Lakshmi K and Mohan Rao AR (2018) Dynamic force reconstruction techniques from incomplete measurements. *Journal of Vibration and Control* 24(22): 5321–5344.

Jiang H, Liu W, Huang H, et al. (2022) Parametric design of developable structure based on Yoshimura origami pattern. *Sustainable Structures* 2(2): 000019.

Kaveh A, Dadras Eslamlou A, Rahmani P, et al. (2022) Optimal sensor placement in large-scale dome trusses via Q-learning-based water strider algorithm. *Structural Control and Health Monitoring* 29(7): e2949.

Kim J, Jin X, Sohn YW, et al. (2014) Tumoral RANKL activates astrocytes that promote glioma cell invasion through cytokine signaling. *Cancer Letters* 353(1-2): 194–200.

Law SS, Li J and Ding Y (2011) Structural response reconstruction with transmissibility concept in frequency domain. *Mechanical Systems and Signal Processing* 25(3): 952–968.

Li J and Hao H (2014) Substructure damage identification based on wavelet-domain response reconstruction. *Structural Health Monitoring* 13(4): 389–405.

Li YX and Sun LM (2024) Substructure-level damage identification based on the spectrum-probability space of the transmissibility function. *Journal of Sound and Vibration* 571: 118117.

Li J, Law SS and Ding Y (2012) Substructure damage identification based on response reconstruction in frequency domain and model updating. *Engineering Structures* 41: 270–284.

Li J, Law SS and Hao H (2013) Improved damage identification in bridge structures subject to moving loads: numerical and experimental studies. *International Journal of Mechanical Sciences* 74: 99–111.

Li Z, Hou J and Jankowski Ł (2022) Structural damage identification based on estimated additional virtual masses and Bayesian theory. *Structural and Multidisciplinary Optimization* 65(2): 45.

Liu K, Law SS and Zhu XQ (2015) Substructural condition assessment based on force identification and interface force sensitivity. *International Journal of Structural Stability and Dynamics* 15(02): 1450046.

Liu C, Zhang PN and Xu XB (2023) Literature review of digital twin technologies for civil infrastructure. *Journal of Infrastructure Intelligence and Resilience* 2(3): 100050.

Ni PH, Li Q, Han Q, et al. (2023) Substructure approach for Bayesian probabilistic model updating using response reconstruction technique. *Mechanical Systems and Signal Processing* 183: 109624.

Venkata Rao R (2016) Jaya: a simple and new optimization algorithm for solving constrained and unconstrained optimization problems. *International Journal of Industrial Engineering Computations* 7(1): 19–34.

Reich GW and Park KC (2001) A theory for strain-based structural system identification. *Journal of Applied Mechanics* 68(4): 521–527.

Ritto TG and Rochinha FA (2021) Digital twin, physics-based model, and machine learning applied to damage detection in structures. *Mechanical Systems and Signal Processing* 155: 107614.

Sun H and Betti R (2014) Simultaneous identification of structural parameters and dynamic input with incomplete output-only measurements. *Structural Control and Health Monitoring* 21(6): 868–889.

Sun H and Büyüköztürk O (2015) Identification of traffic-induced nodal excitations of truss bridges through heterogeneous data fusion. *Smart Materials and Structures* 24(7): 075032.

Tao F, Zhang H, Liu A, et al. (2018) Digital twin in industry: state-of-the-art. *IEEE Transactions on Industrial Informatics* 15(4): 2405–2415.

Tee KF, Koh CG and Quek ST (2009) Numerical and experimental studies of a substructural identification strategy. *Structural Health Monitoring* 8(5): 397–410.

Teng S, Chen XD, Chen GF, et al. (2023) Structural damage detection based on transfer learning strategy using digital twins of bridges. *Mechanical Systems and Signal Processing* 191: 110160.

Torzoni M, Tezzele M, Mariani S, et al. (2024) A digital twin framework for civil engineering structures. *Computer Methods in Applied Mechanics and Engineering* 418: 116584.

Wang M, Wang C, Hnydiuk-Stefan A, et al. (2021) Recent progress on reliability analysis of offshore wind turbine support structures considering digital twin solutions. *Ocean Engineering* 232: 109168.

Wang M, Feng S, Incecik A, et al. (2022) Structural fatigue life prediction considering model uncertainties through a novel digital twin-driven approach. *Computer Methods in Applied Mechanics and Engineering* 391: 114512.

Wang M, Incecik A, Feng S, et al. (2023) Damage identification of offshore jacket platforms in a digital twin framework considering optimal sensor placement. *Reliability Engineering & System Safety* 237: 109336.

Weng S, Zhu H, Xia Y, et al. (2020) A review on dynamic substructuring methods for model updating and damage

detection of large-scale structures. *Advances in Structural Engineering* 23(3): 584–600.

Wilt J, Liang R, GangaRao H, et al. (2023) Structural responses of FRP sheet piles under cantilever loading. *Sustainable Structures* 3(1): 000021.

Yang K, Ding Y, Geng F, et al. (2023) A multi-sensor mapping Bi-LSTM model of bridge monitoring data based on spatial-temporal attention mechanism. *Measurement* 217: 113053.

Yu Y, Li J, Li J, et al. (2023) Automated damage diagnosis of concrete jack arch beam using optimized deep stacked autoencoders and multi-sensor fusion. *Developments in the Built Environment* 14: 100128.

Zhang CD and Xu YL (2016) Structural damage identification via multi-type sensors and response reconstruction. *Structural Health Monitoring* 15(6): 715–729.

Zhang CD and Xu YL (2017) Multi-level damage identification with response reconstruction. *Mechanical Systems and Signal Processing* 95: 42–57.

Zhang Z, Koh CG and Duan WH (2010) Uniformly sampled genetic algorithm with gradient search for structural identification–Part I: global search. *Computers & Structures* 88(15-16): 949–962.

Zhang S, Wang Z, Jian Z, et al. (2020) A two-step method for beam bridge damage identification based on strain response reconstruction and statistical theory. *Measurement Science and Technology* 31(7): 075008.

Zhang GC, Wan CF, Xiong XB, et al. (2022) Output-only structural damage identification using hybrid Jaya and differential evolution algorithm with reference-free correlation functions. *Measurement* 199: 111591.

Zhang GC, Wan CF, Xie LY, et al. (2023a) Structural damage identification with output-only measurements using modified Jaya algorithm and Tikhonov regularization method. *Smart Structures and Systems* 31(3): 229–245.

Zhang GC, Wan CF, Xue ST, et al. (2023b) A global-local hybrid strategy with adaptive space reduction search method for structural health monitoring. *Applied Mathematical Modelling* 121: 231–251.

Zhu HP, Mao L and Weng S (2014) A sensitivity-based structural damage identification method with unknown input excitation using transmissibility concept. *Journal of Sound and Vibration* 333(26): 7135–7150.

Zhu ZM, Zhu SY, Wang YW, et al. (2023) Structural dynamic response reconstruction with multi-type sensors, unknown input, and rank deficient feedthrough matrix. *Mechanical Systems and Signal Processing* 187: 109935.

Zou Y, Lu X, Yang J, et al. (2022) Structural damage identification based on transmissibility in time domain. *Sensors* 22(1): 393.